KSCE Journal of Civil Engineering (2018) 22(8):2776-2783

DOI 10.1007/s12205-017-1469-x

Geotechnical Engineering

pISSN 1226-7988, eISSN 1976-3808
www.springer.com/12205

Determination of Maximum Penetration Depth of Suction Caissons in Sand

Wu Yuqi*, LI Dayong, Zhang Yukun***, and Chen Fuquan******

Received August 31, 2016/Revised March 19, 2017/Accepted August 16, 2017/Published Online November 6, 2017

Abstract

The suction caisson is a large top-closed cylindrical steel structure in diameter, short in length and much thinner in skirt wall thickness. The total resistance of the suction caisson during installation consists of the tip resistance and the skirt wall friction. However, since the thickness of the skirt wall is very small, the skirt wall friction may produce additional vertical stress and shear stress in soil at the skirt tip level, and this additional vertical stress and shear stress will contribute to the increase in the skirt tip resistance. At the same time, seepage induced by suction also causes the tip resistance to reduce significantly. A modified slip-line field is proposed in this study estimating the tip resistance in terms of the slip-line theory. The expression obtaining the minimum suction to install the suction caisson is also proposed in terms of the force equilibrium. In addition, the critical suction is determined based on the mechanism of sand piping. Thus, the maximum penetration depth of the suction caisson can be reached when the critical suction equals the minimum suction. Results from calculations of the minimum suction and the maximum penetration depth have been proved to be in a good agreement with the measured data.

Keywords: *suction caisson, suction installation, sand, slip-line method, tip resistance, maximum penetration depth*

1. Introduction

Suction caissons have been increasingly used to act as foundations for offshore wind turbines due to easy installation, reuse and saving-cost (Bye *et al*., 1995; Tjelta, 1995; Andersen *et al*., 2005; Jostad and Andersen, 2006; Ibsen, 2008). A suction caisson is open at the bottom and closed at the top, like an upturned bucket. It first penetrates the seabed to a certain depth under its self-weight with outlet valves on the top open to make water inside the caisson escape. Suction is then produced by pumping out water encased with all outlet valves closed, driving the suction caisson to penetrate to the designed embedded depth. The results from model tests and field installations of suction caissons have proved that the installation under suction is extremely effective in fine- or medium-sized sands, primarily due to reduction in resistance resulting from seepage (Hogervorst, 1980; Tjelta *et al*., 1986; Erbrich *et al*., 1999; Zhang *et al.*, 2004; Andersen *et al.*, 2008). But a more challenging task is to estimate the required suction accurately during installation. Thus, many methods estimating the penetration resistance and the required suction considering reductions in internal friction and end bearing were proposed (Erbrich and Tjelta, 1999; Houlsby and Byrne, 2005; Andersen *et al.*, 2008). Li *et al*. (2013) set up a linear relationship between the required suction and the penetration depth by using the energy principle, incorporating tip resistance calculated using the bearing capacity equation.

Normally, the skirt tip resistance can be calculated in terms of the bearing capacity theory, in which the effective overburden is assumed to be $q = \gamma' z$. But in the case of the long skirt length relative to the skirt wall thickness, the skirt wall friction may produce an important additional vertical stress and shear stress in soil at skirt tip level. This additional vertical stress and shear stress will contribute to the increase in the skirt tip resistance. However, only the increase in skirt tip resistance caused by additional vertical stress in soil at the skirt tip level was considered (Clausen, 1998; Houlsby and Byrne, 2005; Andersen *et al.*, 2008). The increase in skirt tip resistance resulted from shear stress in soil at the skirt tip level was not taken into consideration, and this will underestimate the tip resistance during installation.

The slip-line method is adopted to derive an analytical solution to the tip bearing capacity, in which the increase in skirt tip resistance caused by additional vertical stress and shear stress in soil are considered. The total resistance during installation is calculated as the sum of the friction along outside and inside of the skirt wall and the tip resistance. Installation of the suction caisson is significantly dependent on the minimum suction and the critical suction. The minimum suction is obtained by using the vertical force equilibrium of the caisson. The critical suction is determined by using the mechanism of

*Graduate Student, College of Civil Engineering, Fuzhou University, Fuzhou, Fujian 350116, China (E-mail: 874993277@qq.com)
**Professor, College of Civil Engineering, Fuzhou University, Fuzhou, Fujian 350116, China (Corresponding Author, E-mail: ldydy@163.com)
***Ph.D. Candidate, College of Civil Engineering, Fuzhou University, Fuzhou, Fujian 350116, China (E-mail: philc007@163.com)
****Professor, College of Civil Engineering, Fuzhou University, Fuzhou, Fujian 350116, China (E-mail: phdchen@fzu.edu.cn)

sand piping inside the caisson. Thus, the maximum penetration depth of the caisson is determined in terms of the critical and minimum suctions.

2. Suction Calculation

2.1 Critical Suction Pressure p_{cr}

Suction can significantly reduce the internal friction and the tip resistance, inducing seepage in sand. However, the magnitude of suction must be controlled to avoid the formation of piping channels around the caisson wall, which may cause the installation to stop (Harireche *et al.*, 2013). Andersen *et al.* (2008) assumed that the penetration resistance for an under pressure giving a critical gradient can be estimated by assuming that the inside skirt friction and the tip resistance are reduced to zero when the critical gradient is reached. Thus, the penetration resistance is given by the friction along the outside skirt wall only.

The distribution of pore pressures along inside and outside of the caisson wall is assumed to be linear with the caisson embedded depth (Houlsby and Byrne, 2005). Then the average hydraulic gradients inside and outside the caisson can be expressed as $i_i = (1-a)p/h$ and $i_o = ap/h$, where a is the head loss ratio outside the caisson, p is the suction pressure and h is the penetration depth. When the critical suction pressure p_{cr} is reached, the vertical effective stress inside the skirt reduces to zero, and then we have

$$\gamma' h - (1-a)p_{cr} = 0 \tag{1}$$

Thus,

$$p_{cr} = \frac{\gamma' h}{1-a} \tag{2}$$

During installation of the suction caisson in sand, the soil inside the caisson may be loosened due to the upward water flow caused by the applied suction pressure. Houlsby and Byrne (2005) suggested that some loosening of the sand within the caisson arises due to the upward flow of water. CPT tests conducted inside the caisson before and after installation revealed the significant loosening of sand inside the caisson (Tran *et al.*, 2005; Kim *et al.*, 2016). The looser soil will cause an increase in the permeability and change the distribution of seepage gradients (Erbrich and Tjelta, 1999). For simplicity, one can consider a permeability k_o for the soil outside the caisson and k_i for the soil inside the caisson, and the ratio $k_f = k_i/k_o$. Houlsby and Byrne (2005) suggested that the effects of different k_f values can be accounted for in Eq. (3):

$$a = \frac{a_1 k_f}{1+(k_f-1)a_1} \tag{3}$$

where $a_1 = 0.45-0.36[1-\exp(-2.08h/D)]$. Eq. (3) shows that the head loss within the caisson is reduced in an inverse proportion to the permeability. In this paper, for simplicity, the values of factor a can be calculated by

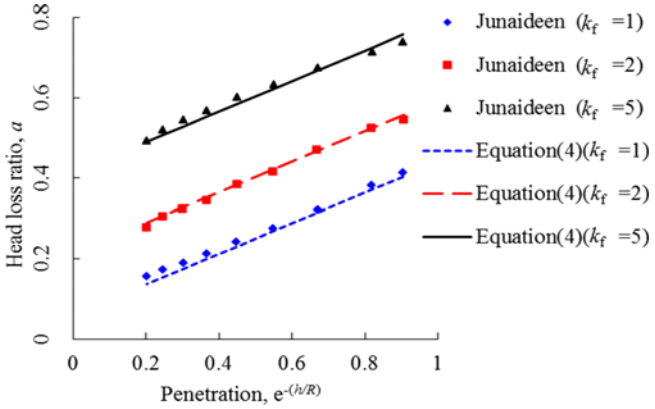

Fig. 1. Variations of Head Loss Ratio a with $e^{-(h/R)}$ and k_f

$$a = 0.06 + 0.22\ln(k_f) + 0.38e^{\left(-\frac{h}{R}\right)} \tag{4}$$

Figure 1 shows a comparison between calculated factors using Eq. (4) and the numerical results proposed by Houlsby and Byrne (2005).

Harireche *et al.* (2014) suggested that k_f should increase during the suction caisson installation, indicating that the soil inside the caisson to become looser continuously. Kim *et al.* (2016) proved that the values of factor a calculated from the centrifuge test results decrease as the skirt penetration progresses, and its variation tendency shows a similar trend with the results obtained by Eq. (3) when $k_f = 2$ to 3.

Substituting Eq. (4) into Eq. (2) produces the following expression of critical suction that can be used to judge whether piping failure occurs inside the caisson.

$$p_{cr} = \frac{\gamma' h}{0.94 - 0.22\ln(k_f) - 0.38e^{\left(-\frac{h}{R}\right)}} \tag{5}$$

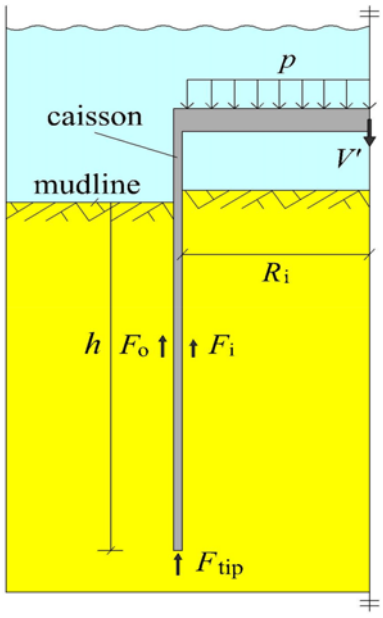

Fig. 2. Equilibrium of Suction Caisson

2.2 Minimum Suction Pressure p_{min}

Suction caisson will encounter the penetration resistance (including friction along inside the skirt wall F_i, friction along outside the skirt wall F_o, and the tip resistance F_{tip}), and the penetration force (suction F_p and effective self-weight of caisson V') during installation (Fig. 2). When the suction force reduces to a minimum value, we have

$$F_p + V' - F_o - F_i - F_{tip} = 0 \tag{6}$$

2.2.1 Suction F_p

The suction F_p can be given as

$$F_p = p\pi R_i^2 \tag{7}$$

2.2.2 Vertical stress of soil at depth z

As shown in Fig. 3, the vertical stress at depth z should be enhanced by the friction along inside of skirt wall during installation.

From Fig. 3, we have

$$\frac{d\sigma_z'}{dz} = \gamma' - i_i\gamma_w + \sigma_z'\frac{(2K\tan\delta)}{R_i} \tag{8}$$

Letting $I_i = \frac{R_i}{2K\tan\delta}$, Eq. (8) becomes

$$\frac{d\sigma_z'}{dz} - \frac{\sigma_z'}{I_i} = \gamma' - i_i\gamma_w \tag{9}$$

which has the solution

$$\sigma_z' = (\gamma' - i_i\gamma_w)I_i(e^{z/I_i} - 1) \tag{10}$$

Similarly, the vertical stress outside the caisson at depth z can be expressed as

$$\sigma_z' = (\gamma' + i_o\gamma_w)I_o(e^{z/I_o} - 1) \tag{11}$$

2.2.3 Friction Along Outside of Skirt Wall

From Eq. (11), the resistance along the outside of the skirt wall F_o can be expressed as

$$F_o = \int_0^h \int_0^{2\pi} \sigma_z' K\tan\delta \cdot R_o \, d\theta' dz = K\tan\delta \cdot 2\pi R_o(\gamma' + \frac{ap}{h})I_o^2(e^{h/I_o} - 1 - h/I_o) \tag{12}$$

2.2.4 Friction Along Inside of Skirt Wall

Similarly, from Eq. (10), the resistance on the inside of the skirt wall F_i can be given as

$$F_i = \int_0^h \int_0^{2\pi} \sigma_z' K\tan\delta \cdot R_i \, d\theta' dz = K\tan\delta \cdot 2\pi R_i(\gamma' - \frac{(1-a)p}{h})I_i^2(e^{h/I_i} - 1 - h/I_i) \tag{13}$$

2.2.5 Tip Resistance

The tip resistance F_{tip} can be expressed as

$$F_{tip} = 2\pi t R_m \sigma_{tip} \tag{14}$$

In the case of a shallow foundation the shearing strength of the overburden is ignored and its weight is only taken into account as an equivalent surcharge $\gamma' h$ (Meyerhof, 1951). σ_{tip} can be then expressed as the sum of terms N_q and N_γ given by Terzaghi (1943). However, the Terzaghi's method may be conservative because it only takes the contribution of the equivalent surcharge rather than shear stress in soil at the skirt tip level to the tip resistance into account. To obtain the accurate tip resistance, a modified slip-line field is proposed, as shown in Fig. 4, the common boundary CE between zones III and IV forms an angle of ω from x direction, and this modified slip-line field can be divided into four distinct zones: active zone I, transition zone II, passive zone III and zone IV.

Currently, the limit equilibrium differential equations of the slip-line will be obtained in terms of the stress equilibrium and yield criterion, whereas only the exact solution to 2-D problems with weightless soil is obtained by the limit analytic methods (Hu *et al.*, 2015). In addition, the displacement pattern of soil around the skirt tip may be closer to plane strain rather than to

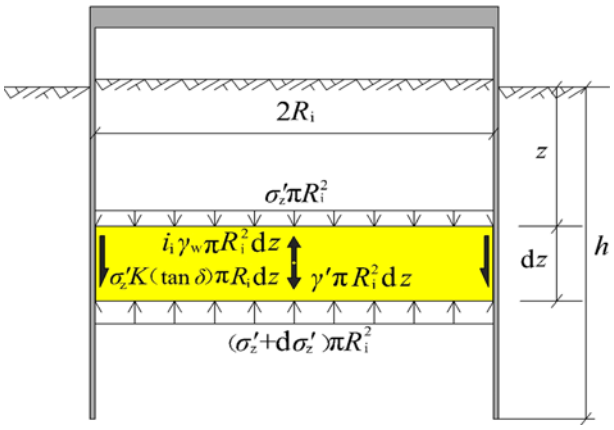

Fig. 3. Equilibrium Condition of Soil at Depth z

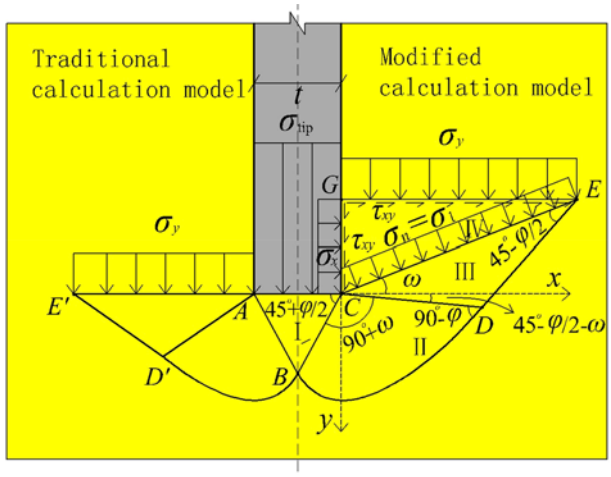

Fig. 4. Comparison between the Traditional and the Modified Models Obtaining the Tip Resistance

axis-symmetry as the skirt wall is thin compared to the skirt diameter (Andersen *et al.*, 2008).

Self-weight and cohesion of soil in plastic area (zone *ABDECA* in Fig. 4) and overburden acting on *CE* can be calculated individually to obtain the total bearing capacity by superposition. However, due to the very thin skirt wall, plastic area will become so small. Therefore, self-weight of sand in this plastic area is too little that the resulted bearing capacity may be ignored. In addition, the cohesion of sand approaches zero so that its contribution to the bearing capacity may also be neglected. The bearing capacity resulted from overburden σ_n is determined as follows.

(1) Basic equations

The following assumptions must be made to calculate the tip resistance using the slip-line method.

① The skirt base is assumed totally smooth.

② Friction angle φ and the lateral earth pressure coefficient of soil K keep constant during the installation.

③ Soil is isotropic and ideally rigid-plastic, obeying Mohr-Coulomb yield criterion, and its weight and volumetric deformation are ignored.

Referring to the coordinate system as shown in Fig. 5, we have the following two equations of equilibrium under conditions of plane strain

$$\left.\begin{aligned}\frac{\partial \sigma_x}{\partial x}+\frac{\partial \tau_{xy}}{\partial y}=0\\ \frac{\partial \tau_{xy}}{\partial x}+\frac{\partial \sigma_y}{\partial y}=0\end{aligned}\right\} \tag{15}$$

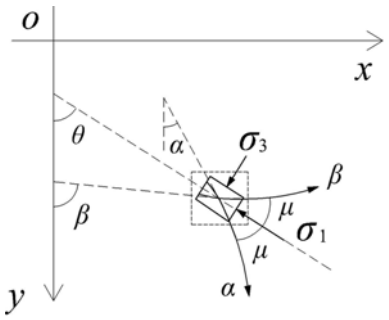

Fig. 5. Coordinate System and Stress Characteristic Lines for Plane Strain Problem

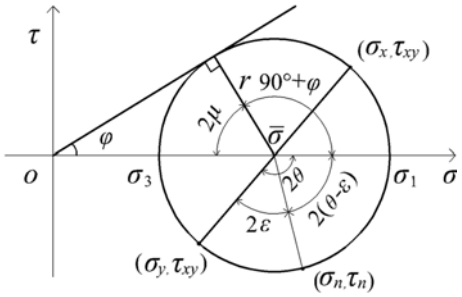

Fig. 6. Mohr-Coulomb Yield Condition for Sand

If a point is in the plastic state, the stress Mohr circle touches the failure envelope of sand as shown in Fig. 6.

Then the stresses can be expressed as

$$\left.\begin{aligned}\sigma_x&=\bar{\sigma}+r\cos 2\theta\\ \sigma_y&=\bar{\sigma}-r\cos 2\theta\\ \tau_{xy}&=r\sin 2\theta\end{aligned}\right\} \tag{16}$$

where $\bar{\sigma}=(\sigma_x+\sigma_y)/2$; $r=\bar{\sigma}\sin\varphi$

Substituting Eq. (16) into Eq. (15) yields

$$\left.\begin{aligned}&\frac{\partial\bar{\sigma}}{\partial x}\sin\varphi\sin 2\theta+\frac{\partial\bar{\sigma}}{\partial y}(1+\sin\varphi\cos 2\theta)\\ &\quad+2r\left(\frac{\partial\theta}{\partial x}\cos 2\theta-\frac{\partial\theta}{\partial y}\sin 2\theta\right)=0\\ &\frac{\partial\bar{\sigma}}{\partial y}\sin\varphi\sin 2\theta+\frac{\partial\bar{\sigma}}{\partial x}(1-\sin\varphi\cos 2\theta)\\ &\quad+2r\left(\frac{\partial\theta}{\partial y}\cos 2\theta+\frac{\partial\theta}{\partial x}\sin 2\theta\right)=0\end{aligned}\right\} \tag{17}$$

Equation (17) that may be solved by using the so-called method of characteristics (Hill, 1950) leads to

$$\begin{cases}\mathrm{d}\bar{\sigma}-2\bar{\sigma}\tan\varphi\cdot\mathrm{d}\theta=0 & \text{along an } \alpha\text{-line}\\ \mathrm{d}\bar{\sigma}+2\bar{\sigma}\tan\varphi\cdot\mathrm{d}\theta=0 & \text{along a } \beta\text{-line}\end{cases} \tag{18}$$

By integration of Eq. (18), the stress characteristic equations along α and β lines can be obtained as

$$\begin{cases}\ln\bar{\sigma}-2\theta\tan\varphi=C_\alpha & \text{along an } \alpha\text{-line}\\ \ln\bar{\sigma}+2\theta\tan\varphi=C_\beta & \text{along a } \beta\text{-line}\end{cases} \tag{19}$$

where C_α and C_β are constants along α and β lines.

From Fig. 4 and Eq. (19), points B and D on the same slip line, thus

$$\ln\bar{\sigma}_B+2\theta_B\tan\varphi=\ln\bar{\sigma}_D+2\theta_D\tan\varphi \tag{20}$$

where $\bar{\sigma}_B$, $\bar{\sigma}_D$ are mean stress at points B and D; θ_B and θ_D are the formed angle of major principle stress from y direction at points B and D, respectively.

What we need to do in the next step is to determine the values of ($\bar{\sigma}$, θ) of points B and D from the given stress boundary

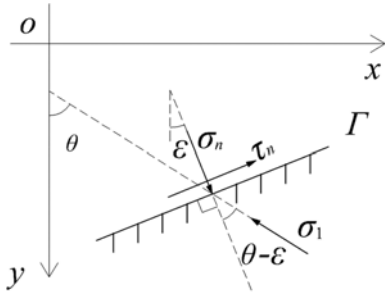

Fig. 7. Stress Boundary Condition

conditions.

(2) Stress boundary conditions analysis

As shown in Fig. 7, consider a boundary Γ whose normal forms an angle of ε from y direction. On the boundary, the normal stress and shear stress are known as σ_n and τ_n.

From Figs. 5 and 6, it has

$$\begin{cases} 2\mu = \pi/2 - \varphi \\ \alpha = \theta - \mu \\ \beta = \theta + \mu \end{cases} \tag{21}$$

The stress over boundary Γ should obey the yield condition. From Fig. 6 and Fig. 7, it has

$$\begin{cases} \sigma_n = \bar{\sigma} + r\cos 2(\theta - \varepsilon) \\ \tau_n = r\sin 2(\theta - \varepsilon) \end{cases} \tag{22}$$

From Eq. (22), $\bar{\sigma}$ and θ can be solved in terms of the given values of σ_n, τ_n and ε:

$$\begin{cases} \bar{\sigma} = \sigma_n - r\cos 2(\theta - \varepsilon) \\ \theta = \varepsilon + \dfrac{1}{2}\arcsin(\dfrac{\tau_n}{r}) \end{cases} \tag{23}$$

(3) Construction of slip line field

① Zone IV

For simplicity, the vertical stress σ_y of soil in this zone is assumed to be the same. Then, from Eq. (10), the expression of σ_y can be given by

$$\sigma_y = \sigma'_i|_{z=h} = (\gamma' - \frac{(1-a)p}{h})I_i(e^{h/I_i} - 1) \tag{24}$$

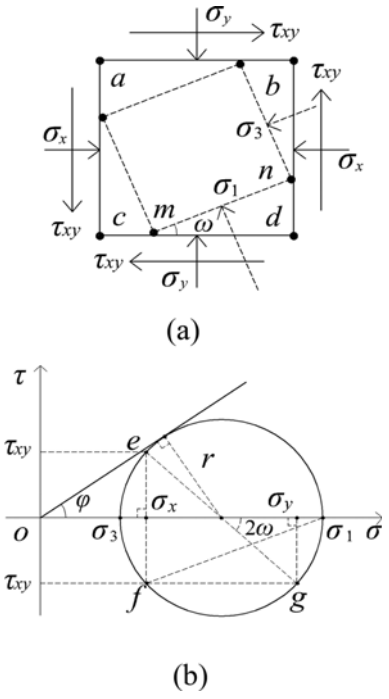

Fig. 8. Stress States of Soil on the Boundary *CE*: (a) Direction of Principle Stresses, (b) Stress States at Failure

Thus, the shear stress of soil can be expressed as

$$\begin{aligned} \tau_{xy} &= \sigma_y K\tan\delta \\ &= (\gamma' - \frac{(1-a)p}{h})I_i(e^{h/I_i} - 1)K\tan\delta \end{aligned} \tag{25}$$

Figure 8(a) shows the direction of principle stresses on the boundary *CE*, and the major principle plane *mn* forms an angle of ω from x direction. Fig. 8(b) shows the ultimate stress state of soil on the boundary *CE*, points *e* and *g* stand for the stress states of soil on the plane *ac* and *ab*, respectively.

Although soil in zone IV does not reach the critical condition, the shear strength on common boundary *CE* develops fully. Thus, from Fig. 8(b), the major principle stress σ_1 can be expressed as

$$\begin{aligned} \sigma_1 &= \sigma_y + r - \frac{(\sigma_y - \sigma_x)}{2} = \frac{(1+K)}{2}\sigma_y(1+\sin\varphi) \\ &= \frac{(1+K)}{2}(1+\sin\varphi)(\gamma' - \frac{(1-a)p}{h})I_i(e^{h/I_i} - 1) \end{aligned} \tag{26}$$

In addition, the value of ω can be derived as

$$\omega = \frac{1}{2}\arctan(\frac{2\tau_{xy}}{\sigma_y - \sigma_x}) = \frac{1}{2}\arctan\frac{2K\tan\delta}{|1-K|} \tag{27}$$

② Passive zone III

In this zone, as shown in Fig. 4, σ_n acting on the boundary *CE* is regarded as the equivalent overload. Then, the normal σ_n and shear stress τ_n acting on the boundary *CE* can be shown as

$$\begin{cases} \sigma_n = \sigma_1 \\ \tau_n = 0 \end{cases} \tag{28}$$

Soil in this zone has a tendency moving up under the driven by σ_{tip}, thus σ_n should be the minor principle stress. Hence, the major principle stress forms an angle of ε from y axis can be expressed as

$$\varepsilon = \frac{\pi}{2} + \omega \tag{29}$$

Combining Eqs. (21), (23), (28) and (29), we get

$$\begin{cases} \theta = \varepsilon = \dfrac{\pi}{2} + \omega = \dfrac{\pi}{2} + \dfrac{1}{2}\arctan(\dfrac{2K\tan\delta}{|1-K|}) \\ \alpha = \dfrac{1}{2}\arctan(\dfrac{2K\tan\delta}{|1-K|}) + \dfrac{\pi}{4} + \dfrac{\varphi}{2} \\ \beta = \dfrac{1}{2}\arctan(\dfrac{2K\tan\delta}{|1-K|}) + \dfrac{3\pi}{4} - \dfrac{\varphi}{2} \\ \bar{\sigma} = \dfrac{\sigma_1}{1-\sin\varphi} \end{cases} \tag{30}$$

Equation (30) shows that θ, α, β and $\bar{\sigma}$ are constant. Thus, we can obtain

$$\bar{\sigma}_D = \bar{\sigma} = \frac{\sigma_1}{1-\sin\varphi} \tag{31}$$

③ Active zone I

In this zone, as shown in Fig. 4, the normal stress σ_n and shear stress τ_n acting on the boundary AC can be shown as

$$\begin{cases}\sigma_n = \sigma_{tip} \\ \tau_n = 0\end{cases} \tag{32}$$

Soil in this zone has a tendency moving down under the action of σ_{tip}. Hence σ_n is the major principle stress, and σ_n forms an angle of ε from y direction can be expressed as

$$\varepsilon = 0 \tag{33}$$

Combining Eqs. (21), (23), (32) and (33), we get

$$\begin{cases}\theta = \varepsilon = 0 \\ \alpha = -(\dfrac{\pi}{4} - \dfrac{\varphi}{2}) \\ \beta = \dfrac{\pi}{4} - \dfrac{\varphi}{2} \\ \bar{\sigma} = \dfrac{\sigma_{tip}}{1+\sin\varphi}\end{cases} \tag{34}$$

Equation (34) proves that θ, α, β and $\bar{\sigma}$ are constant. Then we can get

$$\bar{\sigma}_B = \bar{\sigma} = \frac{\sigma_{tip}}{1+\sin\varphi} \tag{35}$$

④ Transition zone II

According to the properties of slip line field, if slip line field on both sides are known, then the slip line field between them can be determined uniquely. Since active zone I and passive zone III have been proved to be the uniform stress field, thus the slip line of α family are straight and meet at a point, those of the other family should be logarithmic arcs. Fig. 4 gives the slip-line fields for the traditional and the modified methods of obtaining the tip resistance. ω is the angle between boundary CE and x axis, as shown in Fig. 4. It can be found that when ω equals 0, the modified model reduces to the traditional model.

(4) Solution of tip stress

Substituting Eqs. (31) and (35) into Eq. (20) yields

$$\sigma_{tip} = \sigma_1 \frac{1+\sin\varphi}{1-\sin\varphi} \cdot e^{(\pi+2\omega)\cdot\tan\varphi} \tag{36}$$

Combining Eqs. (14), (26) and (36), we obtain

$$F_{tip} = \pi R_m t(1+K)(\gamma' - \frac{(1-a)p}{h}) I_i (e^{h/I_i} - 1) \frac{(1+\sin\varphi)^2}{1-\sin\varphi} e^{(\pi+2\omega)\cdot\tan\varphi} \tag{37}$$

For conventional caissons, the thickness of skirt wall is far smaller than radius, i.e. $t \ll R$, thus $R_i \approx R_o \approx R_m = R$ and $I_i \approx I_o = I$.

Substituting Eqs. (7), (12), (13) and (37) into Eq. (6) yields

$$p_{min} = \frac{(1+K)I(e^{h/I}-1)M\gamma' t + 4\gamma' NK\tan\delta - V'/(\pi R)}{R - \{2NK\tan\delta - [(1+K)I(e^{h/I}-1)tM + 4NK\tan\delta](1-a)\}/h} \tag{38}$$

where $M = \dfrac{(1+\sin\varphi)^2}{1-\sin\varphi} \cdot e^{(\pi+2\omega)\cdot\tan\varphi}$; $N = I^2(e^{h/I} - 1 - h/I)$.

3. Theoretical Formula Validation

We borrow the measured results from both field installation (cited in Houlsby and Byrne, 2005) and centrifuge model installation (Kim *et al.*, 2016) to validate the proposed theoretical methods. In all calculations, the lateral earth pressure coefficient of $K = 0.8$ is used, which is recommended by API (1993) for the calculation of drained shaft friction of open-ended unplugged piles.

3.1 Trial Installation at Tenby

At Tenby, a field test with a caisson of 2 m diameter, 2 m height and a wall thickness of 8 mm was performed in dense sand. Dimensions of the caisson and physical parameters of the soil are shown in Table 1.

Figure 9 presents the comparison between calculated results and measured data. It can be found that the measured suction increases approximately linearly with penetration depth up to the full penetration 1.4 m; the minimum suction predicted is in a good agreement with the measured data. In addition, the critical suction curve intersects the minimum suction curve at a point, where installation of the caisson will be terminated, because the higher suction will lead to sand piping inside the caisson and the lower suction may unable to overcome the penetration resistance. As shown in Fig. 9, in the final stage of installation, the measured suction is greater than critical suction predicted, and this will result in sand piping inside the caisson, leading to terminating the installation of caisson at 1.4 m deep.

3.2 Trial installation at Sandy Haven

At sandy Heaven, the caisson with 4 m × 2.5 m × 20 mm (diameter × height × thickness) was installed in sand. Table 2 shows the dimensions of the caisson and physical parameters of the soil.

Table 1. Data Used for Calculations

Soil	γ' (kN/m^3)	k_f	$K\cdot\tan\delta$	φ(deg)
	8.5	3	0.48	40
Caisson	R(m)	L(m)	t(mm)	V'(kN)
	1	2	8	10

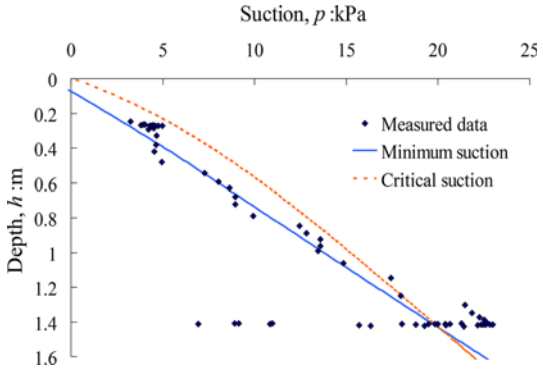

Fig. 9. Suction vs. Penetration Depth

Table 2. Data Used for Calculations

Soil	γ' (kN/m^3)	k_f	$K\cdot\tan\delta$	φ(deg)
	8.5	2	0.48	40
Caisson	R(m)	L(m)	t(mm)	V'(kN)
	2	2.5	20	100

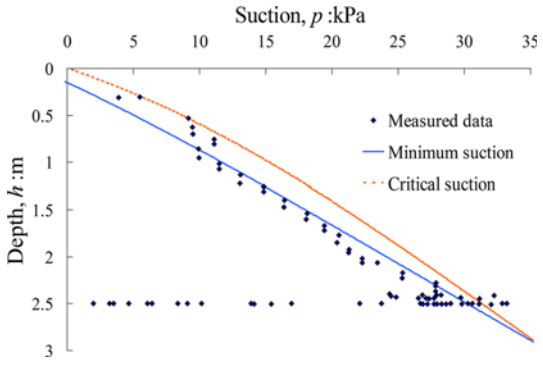

Fig. 10. Suction vs. Penetration Depth

Figure 10 shows the comparison of analytical solution with field installation data. It can be observed that the predicted suction agrees well with the experimental data. Furthermore, both the measured and theoretical calculated suction increase approximately linearly with penetration depth. In addition, the predicted maximum penetration depth is greater than the height of caisson. Thus, the caisson can be eventually installed to its full depth.

3.3 Centrifuge Model Tests

This case reports the centrifuge model test performed by Kim *et al.* (2016). The model caisson with 200 mm × 200 mm × 2 mm (diameter × height × thickness), equivalent to 5 m × 5 m × 50 mm in prototype dimension at 25g, was installed in sand. Dimensions of the model caisson and physical parameters of the soil are given in Table 3. The interface friction angle between aluminum and sand of $\delta = 19$ is adopted as suggested by Tran *et al.* (2008). The penetration of caisson was terminated at 3.8 m due to the lack of water pumping rate.

Figure 11 shows the results of centrifuge model tests and the analytical predictions. Clearly, the theoretical predicted suction is in a good agreement with the centrifuge test data. In addition, the predicted maximum penetration depth is greater than the measured penetration depth of 3.8 m. Thus, the model caisson can be installed successfully.

From Figs. (9) to (11), it is obvious that the measured suction increases approximately linearly with the penetration depth, and

Table 3. Data Used for Calculations

Soil	γ' (kN/m^3)	k_f	K	φ (deg)
	9	2.5	0.8	40
Caisson	R(m)	L(m)	t(mm)	δ(deg)
	2.5	5	50	19

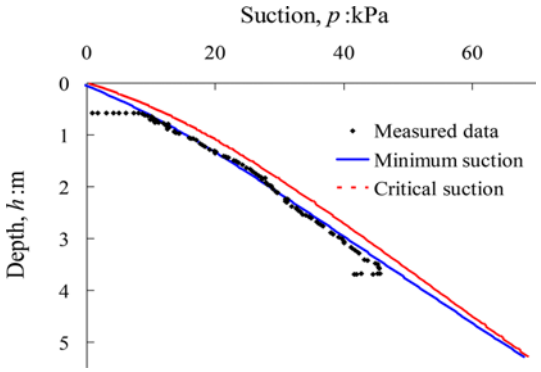

Fig. 11. Suction vs. Penetration Depth

the minimum suction predicted by the proposed method is in a very good agreement with the measured data.

4. Conclusions

The tip resistance of suction caisson is determined by a modified slip-line field in terms of the slip-line theory. To satisfy practical conditions, the proposed method considers the increase in the tip resistance from both the friction along the caisson wall and the shear stress in the soil at the skirt tip level induced by skirt wall friction. The total resistance of the caisson is expressed as the sum of friction along the outside and inside of the skirt wall and tip resistance. The minimum suction is obtained by using the force equilibrium method, and its validity has been proved by using the field and centrifuge model test results. The critical suction is determined by using the mechanism of sand piping. The maximum penetration depth of the caisson is determined when the minimum suction equals critical suction, and the maximum penetration depth agrees well with the measured data.

Acknowledgements

This study was financially supported by the National Science Foundation of China (Grant Nos. 51379118, 51639002) and SDUST Research Fund (Grant No. 2015KYJH104).

Notations

a = Head loss ratio outside the caisson
D = Diameter of the caisson
h = Penetration depth
i = Hydraulic gradient
k = Permeability coefficient
k_f = Ratio of permeability within caisson to outside caisson (i.e. $k_f = k_i/k_o$)
p = Suction pressure
z = Depth below the mudline
R = Radius of the caisson
t = Skirt wall thickness
$\overline{\sigma}$ = Mean stress

r = Radius of Mohr stress circle
N_q, N_γ = Bearing capacity factors
φ = Friction angle of soil
θ' = Angle in the circumferential direction of the caisson
θ = Angle between the direction of the major principle stress and y axis
ω = Angle between the boundary CE and x axis
α, β = Angle between the α or β slip-line and y axis, respectively
μ = Angle between the slip line and the direction of the major principle stress
ε = Angle between the direction of the normal stress and y axis on the boundary Γ

References

American Petroleum Institute (API) (1993). *Recommended practice for planning, designing and constructing fixed offshore platforms,* API RP 2A, American Petroleum Institute, Washington, D.C.

Andersen, K. H., Murff, J. D., Randolph, M. F., Clukey, E. C., Erbrich, C. T., Jostad, H. P., Hansen, M., and Supachawarote, C. (2005). "Suction anchors for deep water applications. Keynote lecture." *In: Proceedings of the International Symposium on Frontiers in Offshore Geotechnics, Perth, Western Australia,* pp. 3-30.

Andersen, K. H., Jostad, H. P., and Dyvik, R. (2008). "Penetration resistance of offshore skirted foundations and anchor in dense sand." *Journal of Geotechnical and Geoenvironmental Engineering*, Vol. 134, No. 1, pp. 106-116, DOI: 10.1061/(ASCE)1090-0241(2008)134:1(106).

Bye, A., Erbrich, C., Rognlien, B., and Tjelta, T. I. (1995). "Geotechnical design of bucket foundations." *In: Proceedings of the Offshore Technology Conference*. *Paper No. OTC 7793.* 27th Ed., pp. 869-883, DOI: 10.4043/ 7793-MS.

Clausen, C. J. F. (1998). "Fundamentering av plattformer; Observasjonerog refleksjoner." *16th Laurits Bjerrum Memorial Lecture*, Norwegian Geotechnical Institute, Oslo.

Erbrich, C. T. and Tjelta, T. I. (1999). "Installation of bucket foundations and suction caissons in sand-geotechnical performance." *Proceedings of the 31th Annual Offshore Technology Conference*, *Houston: OTC 10990*, pp. 725-735. DOI: 10.4043/10990-MS.

Hogervorst, J. R. (1980). "Field trials with large diameter suction piles." *Proc., Offshore Technology Conf., OTC 3817,* 12th Ed., pp. 217-224, DOI: 10.4043/3817-MS.

Houlsby, G. T. and Byrne, B. W. (2005). "Design procedure for installation of suction caissons in sand." *Geotechnical Engineering*, Vol. 158, No. 3, pp.135-144, DOI: 10.1680/geng.2005.158.3.135.

Harireche, O., Mehravar, M., and Alani, A. M. (2013). "Suction caisson installation in sand with isotropic permeability varying with depth." *Applied Ocean Research*, Vol. 43, pp. 256-263, DOI: 10.1016/j.apor.2013.10.008.

Harireche, O., Mehravar, M., and Alani, A. M. (2014). "Soil conditions and bounds to suction during the installation of caisson foundations in sand." *Ocean Engineering*, Vol. 88, pp. 164-173, DOI: 10.1016/j.oceaneng.2014.06.033.

Hu, Z. P., Wang, R., and Xia, X. B. (2015). "Modifying the formula of the ultimate bearing capacity of a shallow circular foundation." *Journal of Highway and Transportation Research and Development*, Vol. 9, No. 1, pp. 1-7, DOI: 10.1061/JHTRCQ.0000419.

Hill, R. (1950). *The Mathematical Theory of Plasticity*, Clarendon Press, Oxford.

Ibsen, L. B. (2008). "Implementation of a new foundations concept for offshore wind farms." *In: Proceedings of the Nordisk Geoteknikermøte Nr. 15. NGM 2008, Sandefjord, Norway,* pp. 19-33.

Jostad, H. P. and Andersen, K. H. (2006). "Potential benefits of using skirted foundations for jack-up platforms." *In: Proceedings of the Offshore Technology Conference. Paper No. OTC 18016,* Houston. DOI: 10.4043/18016-MS.

Kim, D. S., Lee, S. T., and Kim, J. H. (2016). Centrifuge model tests on installation of suction caissons in sand. "*Japanese Geotechnical Society Special Publication*." Vol. 4, No. 4, pp.73-77, DOI: 10.3208/jgssp.v04.k05.

Li, D. Y., Zhang, Y. K., Gao, Y. F., and Song, Y. J. (2012). "Model tests on penetration of suction anchors in medium-coarse sand." *Chinese Journal of Geotechnical Engineering*, Vol. 34, No. 12, pp. 2278-2283. (in Chinese)

Meyerhof, G. G. (1951). "The ultimate bearing capacity of foundations." *Geotechnique*, Vol. 2, No. 4, pp. 301-332, DOI: 10.1680/geot.1951.2.4.301.

Terzaghi, K. (1943). *Theoretical soil mechanics*, New York: Wiley John.

Tjelta, T. I. (1995). " Geotechnical experience from the installation of the europipe jacket with bucket foundations." *In: Proceedings of the Offshore Technology Conference*. Paper No. OTC 7795, DOI: 10.4043/7795-MS.

Tjelta, T. I., Guttormsen, T. R., and Hermstad, J. (1986). "Large scale penetration test at a deepwater site." *Proc., Offshore Technology Conf.*, OTC 5103, 18th Ed., 201-212, DOI: 10.4043/5103-MS.

Tran, M. N., Randolph, M. F., and Airey, D. W. (2005). "Study of seepage flow and sand plug loosening in installation of suction caissons in sand." *Proceedings of the Fifteenth International Offshore and Polar Engineering Conference*, Seoul. pp. 516-521.

Tran, M. N. and Randolph, M. F. (2008). "Variation of suction pressure during caisson installation in sand." *Geotechnique*, Vol. 58, No. 1, pp. 1-11, DOI: 10.1680/geot.2008.58.1.1.

Zhang, S. H., Zheng, Q. A., and Liu, X. A. (2004). "Finite element analysis of suction penetration seepage field of bucket foundation platform with application to offshore oilfield development." *Ocean Engineering*, Vol. 31, pp. 1591-1599, DOI: 10.1016/j.oceaneng.2004.03.001.